OBSERVATIONAL CONSTRAINTS ON THE ATMOSPHERES OF URANUS AND NEPTUNE FROM NEW MEASUREMENTS NEAR 10 μm

Glenn S. Orton[1,4]

Alan T. Tokunaga[2,5]

John Caldwell[3,4]

[1]M.S. 183-301, Jet Propulsion Laboratory,
California Institute of Technology
4800 Oak Grove Drive, Pasadena, CA 91109

[2]Institute for Astronomy, University of Hawaii,
2680 Woodlawn Drive, Honolulu, HI 96822

[3]Department of Earth and Space Science,
State University of New York, Stony Brook, NY 11794

[4]Visiting Astronomer at the Infrared Telescope Facility which is operated by the University of Hawaii under contract from the National Aeronautics and Space Administration

[5]Staff Astronomer at the NASA Infrared Telescope Facility

Running head: Observations of Uranus and Neptune near 10 μm

Editorial Correspondence:

Dr. Glenn S. Orton
Mail Stop 183-301
Jet Propulsion Laboratory
4800 Oak Grove Drive
Pasadena, CA 91109

ABSTRACT

We have made the first detections of Uranus at 10.3, 11.6 and 12.5 μm with approximately 1 μm spectral bandpasses, with respective brightness temperatures of $74.0 \pm {}^{0.9}_{1.1}$, $67.6 \pm {}^{0.5}_{0.7}$ and $65.5 \pm {}^{0.6}_{0.7}$ K and the first detection of Neptune at 10.3 μm with a brightness temperature of $77.5 \pm {}^{0.7}_{0.9}$ K. We also detected Neptune at 11.36 μm with 2% spectral resolution at $81.0 \pm {}^{0.8}_{0.9}$ K. The 10 μm continuum of both Uranus and Neptune may in part be due to reflected solar radiation as well as thermal emission. If all of the observed flux is reflected light, then the maximum geometric albedo of Uranus is 0.115 ± 0.020, and that of Neptune is 0.229 ± 0.043. In the context of previous observations in this region, the maximum stratospheric C_2H_6 mixing ratio is found to be 3×10^{-8} for Uranus and 3×10^{-6} for Neptune. A value for the maximum mixing ratio in the stratosphere of Neptune on the order of $1 - 4 \times 10^{-2}$ appears to be consistent with the available data.

I. INTRODUCTION

Uranus and Neptune have strikingly dissimilar spectra in the 8 to 14 μm region, as first reported by Gillett and Rieke (1977) and by Macy and Sinton (1977). Emission features due to CH_4 at 7 μm and C_2H_6 at 12 μm are evident in the spectrum of Neptune but not Uranus. Part of this difference is undoubtedly due to differences in temperature structure between the two planets, e.g. a hotter stratosphere for Neptune (Tokunaga et al., 1982). Other differences between the two atmospheres are indicated by the shapes of strong 1-3 μm CH_4 bands which indicate greater aerosol scattering for Neptune than for Uranus (Fink and Larson, 1979) and temporal changes in the near infrared flux from Neptune which are probably caused by changes in the aerosol properties (Brown et al., 1981).

Interpretation of the 8 to 14 μm spectral region for Neptune has been limited to the relatively warm stratosphere, owing to the lack of data between 8.5 and 11.5 μm. Far less is known about Uranus: no unambiguous detection between 8 and 17.8 μm has been reported in the literature. The spectrum could be determined by the collision-induced dipole of H_2 as at longer wavelengths (Orton, 1981), by a cloud layer (as could be expected from CH_4 condensation) or by absorption by other molecules. Further, it could be comprised of either thermal or reflected solar radiation. The level of flux at 8 or 12 μm above a continuum spectrum would place strong constraints on the stratospheric vertical distributions of CH_4 or C_2H_6, respectively.

We report in this paper the first unambiguous detections of Uranus in the 10.3 to 12.5 μm region and of Neptune in the 10.3 to 11.4 μm region using a combination of medium bandwidth interference filters and a cooled variable filter (CVF). The observed radiation at 10.3 μm is partially reflected solar radiation and partially thermal emission from the H_2 continuum. Limits on the C_2H_6 and CH_4 mixing ratios are obtained for Uranus and Neptune.

II. OBSERVATIONS

Uranus and Neptune were observed at 19.6 μm and 17.8 μm using the bolometer system at the NASA Infrared Telescope Facility in July 1981. Further observations were made of Uranus at 11.6 and 12.5 μm, as well as observations of both Uranus and Neptune at 10.3 μm using a more sensitive arsenic-doped silicon photoconductor system at the NASA/IRTF in July 1982. These filters have small bandpasses (see Table 1) and their transmission profiles are shown in Figure 1. The effective wavelengths we quote for these filters take into account the wavelength shift under cooling and the small effects of telluric absorption. We also obtained 2% spectral resolution observations of Neptune during the July 1982 run at 10.90 and 11.36 μm, using the IRTF 8 to 14 μm CVF in conjunction with the photoconductor.

Corrections to the monochromatic flux were computed to take into account the different temperatures of the standard star used for the flux calibration and those of Uranus and Neptune (Morrison, 1973; Low and Rieke, 1974). These corrections were less than 3% because of the relatively narrow bandpass of the filters, and they have been applied to the results presented here. Another correction must be made to our data to account for the effects of seeing and diffraction. Even though Uranus had an apparent diameter of 4 arc sec, we used a 6 arc sec diameter aperture for all our observations in order to reduce background noise to an absolute minimum. We calculate a 10% loss of flux from Uranus considering the 2 arc sec seeing conditions which were relatively constant during all the observing runs. No correction of significance was necessary for the Neptune observations since Neptune had an apparent diameter of only 2.3 arc sec.

For all the observations reported here α Bootis (α Boo) served as the primary flux standard and α Scorpii (α Sco) served as a secondary standard.

The absolute flux scale for α Boo is shown in Table 1, and it is consistent with that published by Beckwith et al. (1976).

The observations are summarized in Table 2 in the form of averages for each period of observation. Results from different nights were averaged by weighting according to the inverse square of the standard deviation. This appeared to be a conservative procedure, as both internal consistency and night-to-night consistency were achieved. The final averaged values and best estimates of the uncertainty are also given in Table 2. We use the term geometric albedo in Table 2 and elsewhere in the text; this is not strictly correct, as our observations were not made at zero phase angle. However our calculations show that corrections to zero phase are much smaller than our observational errors, and so we have taken our observations and calculations as good approximations to the geometric albedo.

III. THERMAL EMISSION MODELS

The interpretation of the results is complicated because some of the continuum flux observed may arise from reflected solar radiation from clouds or haze in the atmospheres of Uranus and Neptune. We discuss two possibilities: (1) the 10-μm emission arises from gaseous emission only, and (2) the 10-μm flux is a combination of thermal emission and reflected solar radiation. Further, the models are consistent with existing far infrared data and reasonable cloud albedos insofar as possible.

A. Uranus

The observations of Uranus reported here are illustrated in Fig. 2 together with the upper limits reported by Gillett and Rieke (1977) and our recent 17.8- and 19.6-μm observations (Tokunaga et al., 1983). The detection brightness levels are consistent with the upper limits given by Gillett and Rieke. Fig. 2

also illustrates the brightness temperatures equivalent to the radiance received from a sphere with a lambertian reflecting surface at Uranus' distance from the sun for different characteristic values of the geometric albedo. The systematic increase in brightness temperature with decreasing wavelength is the most striking characteristic of the observations in this region. This is not inconsistent with the increase in solar radiance with decreasing wavelength but does not rule out the possibility that the radiation is entirely thermal in origin. We defer consideration of the role of reflected solar radiation in the spectrum for a later section.

To gain some insight into the physical interpretation of this spectral region we first hypothesize that all the observed radiation is thermal in origin. If this is true then it is far more likely that we are observing the effects of changes in gaseous opacity than changes in cloud emissivity over such a short wavelength range. In fact, the simplest interpretation consistent with purely thermal radiation is that the collision-induced opacity of H_2, probably the dominant atmospheric opacity source in the far infrared (Trafton, 1967; Orton, 1981), also dominates the atmospheric opacity in the 10 - 12-μm region. Gaseous absorption thus rapidly increases toward the center of the S(1) rotation line near 16.7 μm.

1. Temperature Structure

With the above assumption, the radiances observed at 10.3 and 11.6 μm can be used to constrain the thermal structure, reserving the 12.5-μm measurement to estimate the strength of C_2H_6 stratospheric emission. In establishing a model atmosphere calculation for transfer of both thermal and reflected solar radiation, we assumed a bulk composition of 90% H_2 and 10% He and CH_4 by volume. This H_2 mixing ratio value is close to that of Jupiter (89%, Gautier et al., 1981) and Saturn (94%, Gautier et al., 1983). We retained a constant mixing

ratio for H_2 throughout this paper, since the weighting functions for outgoing radiation are relatively constant for various models with different He and CH_4 mixing ratios, and it is not possible to determine the He to H_2 abundance ratio from our data in the 10.3 to 19.6 μm region. For the models in this section, the atmosphere is assumed to be free of absorbing or scattering particles which could influence radiation at these wavelengths. The outgoing radiances were computed by integrating from the 2.5 bar level through the 10^{-5} bar level, the H_2 opacity being important at the high pressures and the CH_4 and C_2H_6 opacities important at the low pressures.

The H_2 collision-induced dipole opacity was computed on the basis of the recent work of Dore et al. (1983) for H_2-H_2 collisions and on the work of Cohen et al. (1983) for H_2-He collisions. An explicit calculation was made for H_2-CH_4 collisions based on data supplied by Birnbaum (unpublished communication), a sample of which is shown in Fig. 3 of Birnbaum (1982). A provisional fit to these data at 195 and 297 K was provided as described in the Appendix. The weighting functions for the 10.3 and 11.6 μm filtered radiances are strongly overlapping, as are those for the 17.8 and 19.6 μm filtered radiances, so only two temperatures can be retrieved in a vertically independent sense. We thus followed a procedure adopted by Tokunaga et al. (1983) and perturbed the temperature structure of a radiative-convective equilibrium model by Appleby (1980). Interpolation of temperature changes between the two independent levels, at 50 and 400 mbar, was made linearly as a function of the logarithm of total pressure.

Another perturbation in temperatures was applied to the stratosphere. As in Tokunaga et al., this perturbation was made at the 2.5 mb total pressure level, with linear interpolation of temperature changes as a function of pressure logarithm between 2.5 and 60 mb. This effectively varies the local lapse rate near 60 mb and changes the difference in the brightness temperatures

characterizing the 17.8 and 19.6 μm filtered radiances. Temperature structure models were considered valid only when the stratospheric temperature perturbations caused the model to produce the same difference in 17.8 vs. 19.6 μm brightness temperatures as observed by Tokunaga et al. The perturbation of temperatures above the 2.5 mb level was arranged to vary linearly with logarithm of pressure so that the 0.1 mb temperature would be fixed at 140 K, consistent with the results of the stellar occultation analysis by Sicardy et al. (1982) and French et al. (1983a).

Below the 400 mb level, we assumed fully convective conditions and used an adiabatic lapse rate to extrapolate to higher pressures. The 400 mb level is approximately consistent with the radiative-convective boundary in the equilibrium models of Appleby (1980) and Wallace (1980). More importantly, we have varied the methane mixing ratio in the deep atmosphere in several models. The variation of the CH_4 mixing ratio produces a variety of lapse rates between 400 mb and 1 bar arising from changes in the vertical extent of the wet adiabat in the region where CH_4 condensation takes place (e.g. Eq. 3 of Wallace, 1980). In all models, the methane atmospheric partial pressure was set equal to the saturation vapor pressure above the condensation level (except in the stratosphere where the mixing ratio was set equal to its value at the temperature minimum). In three different models, the CH_4 mixing ratio in the deep atmosphere was assumed to be (a) 0.2%, close to that of Jupiter, (b) 2%, a somewhat arbitrary "intermediate" value, which is a slightly lower than the value derived by Baines (1983) from analysis of high resolution visual spectrophotometry, and (c) 10%, an extreme upper value first offered by Danielson (1977).

The results of the temperature retrievals are shown in Fig. 3 for each of the three CH_4 mixing ratios assumed in the deep atmosphere. The difference between the wet and dry adiabats in the region of CH_4 condensation are apparent.

Fig. 2 illustrates the 8-20 μm brightness temperature spectrum of each of the models, considering the H_2 collision-induced absorption alone. All the models are constrained to be consistent with the 17.8 and 19.6 μm brightness temperatures from Tokunaga et al. (1982). The shallow spectral feature in the H_2 continuum near 950 cm^{-1} is the rotation line associated with the double transition $S_0 + S_1$ (Bachet et al., 1982). The effect of the shallow lapse rate for the 10% CH_4 mixing ratio case is evident in the spectrum. In fact, this model produces the highest residuals compared to the data, and therefore we do not consider the 10% CH_4 model further in this section. The residuals to the data which result from the 2% and 0.2% tropospheric CH_4 models are much better, and we consider them to be approximately equal quality fits.

For completeness we have also followed an alternative method for modeling the stratospheric temperature structure used by Tokunaga et al. (1982). In this method a linear temperature vs. logarithm of pressure relationship was assumed above the 60 mbar level. Another linear relationship connected the 60 mbar level with the 250 mbar level, below which Appleby's radiative-convective equilibrium model was assumed. This temperature structure was therefore piecewise continuous and based partly on an a priori equilibrium model and partly on ad hoc assumptions; as a matter of descriptive convenience this type of temperature structure will henceforth be referenced as the hybrid model. As in the perturbed equilibrium model described above, changes were made to the temperatures at 60 and 400 mbar, with linear interpolation of temperature changes required at intermediate levels. The slope of the stratospheric temperature structure was changed until a fit to the 17.8 minus 19.6 μm brightness temperature difference was achieved. The result for the 0.2% tropospheric CH_4 mixing ratio model is also plotted in Fig. 3. It is useful to remember that, while the perturbed equilibrium temperature structures appear more realistic,

the available data do not discriminate between them and the more arbitrary hybrid models. The hybrid model spectra are virtually indistinguishable from the perturbed equilibrium model spectra of equivalent CH_4 composition.

2. Minor Constituents

We note that the 12.5 μm filter is not ideal for the purpose of detecting "excess" emission owing to the presence of C_2H_6 in the stratosphere, as the center of the ν_9 C_2H_6 fundamental band is near 12.2 μm. Thus, additional stratospheric emission from C_2H_6 would affect both the 11.6 and the 12.5 μm radiances, although the latter more strongly. However, it is unlikely that unacknowledged C_2H_6 emission at 11.6μm exerted much influence over the recovered atmospheric structure and the resulting H_2 continuum level. Such a systematic error would produce an overestimate of the level of 12.5 μm radiance attributed to H_2 which would actually be due to C_2H_6. In fact, for a given CH_4 tropospheric mixing ratio, the model spectrum resulting were the 11.6 μm radiance measurement ignored would be at most only 0.1 K lower than if it were considered.

With that in mind, Fig. 4 shows the spectra resulting if the C_2H_6 abundance were to be distributed vertically with nothing below the temperature minimum, and the partial pressure equal to the vapor pressure (Ziegler, 1959) in the stratosphere without exceeding the mixing ratios 3×10^{-8}, 1×10^{-8} and 3×10^{-9}, as shown in the figure. The atmospheric model with 0.2% CH_4 was assumed. The atmospheric transmission was computed by a direct integration over C_2H_6 line absorption, using the technique described by Orton (1982). The relevant spectroscopic line parameters for 5373 lines of the ν_9 fundamental were taken from the 1982 GEISA file (Husson et al., 1982) which is based on molecular parameters described by Daunt et al. (1981). The spectra correspond to a triangular filter function with a FWHM equal to 1.5% of the frequency,

and they have been explicitly convolved with the filter functions where appropriate.

Residuals to the data are minimized for the 0.2% tropospheric CH_4 model with a maximum C_2H_6 stratospheric mixing ratio of 1×10^{-8} (see Fig. 4). In a model with 2% CH_4 they are minimized by a maximum C_2H_6 stratospheric mixing ratio of 4×10^{-9}, a lower value than for the 0.2% CH_4 case. The differences between spectra for the perturbed equilibrium models and the hybrid models are less than 0.2 K in brightness temperature.

Our measurements have not provided an extremely critical test of the presence of C_2H_6 in the stratosphere, and we believe the cumulative uncertainties require us merely to state that the maximum C_2H_6 stratospheric mixing ratio is probably below 3×10^{-8}. This upper limit holds if C_2H_6 (1) obeys saturation equilibrium in the lower stratosphere, (2) is not distributed below the temperature minimum level, and (3) is not distributed above the 0.1 mbar level (or if the atmosphere is roughly isothermal above the 0.1 mbar level).

We also show in Fig. 4 the thermal spectrum resulting from the influence of the ν_4 band of CH_4. Direct integration of atmospheric transmission was computed using spectroscopic line parameters described by Orton and Robiette (1980, 1982). The spectra displayed assume a triangular slit fuction with FWHM equal to 1.5% of the frequency.

We distributed CH_4 in the stratosphere according to saturation equilibrium for an upwelling gas, i.e. the mixing ratio is no higher than the minimum value obtained near the temperature minimum. For the perturbed equilibrium model (Fig. 3a) this value is approximately 3×10^{-5}. The resulting absorption feature falls well below the 3 standard deviation upper limit of about 100 K at 8 μm, as determined by Gillett and Rieke (1977). It is therefore possible for more CH_4 to exist in the stratosphere if this criterion is the only one to be

satisfied. However, there is no compelling reason to do so, except purely by analogy with Neptune as described in the following section. Less stratospheric CH_4 would produce insignificant differences from the spectrum shown in Fig. 4.

3. Reflected light

Figs. 2 and 6 clearly show that is is possible to account for the radiance measured from both Uranus and Neptune by reflected solar radiation without appealing to especially-contrived backscattering properties of the atmospheres. For the 1 – 2.5 μm region, the geometric albedo is probably no higher than 0.10 for either planet, due mostly to the strong CH_4 gaseous absorption pervading this spectral region (e.g. Fig. 2a of Fink and Larson, 1979). Even at 5 μm, where CH_4 absorption should be relatively low, the measured geometric albedo is less than 0.002 (Macy et al., 1980; Brown et al., 1981), although other unidentified gaseous absorption could be present.

It would be useful, of course, to know whether models of atmospheric clouds, combined with the known absorption provided by H_2, are capable of explaining the observed radiances. Unfortunately, realistic physical models for cloud properties are not possible. The chief candidate for the upper cloud condensate in both atmospheres is CH_4 ice; while its optical properties are not known in this spectral region, a preliminary absorption spectrum presented by Fink and Sill (1982) in their Fig. 4 shows negligible absorption in the 10–12 μm range.

Instead, we present models using lambertian reflecting surfaces at various atmospheric levels as crude approximations to cloud reflectivities. For completeness, we also include in our model the contribution of thermal radiances. We assumed the temperature structure from the perturbed equilibrium models of Tokunaga et al. (1983) which are substantially lower than those developed in

the last section. The brightness temperature spectra of these models are shown in Fig. 5 for Uranus. The 0.2% CH_4 tropospheric mixing ratio model was used as a baseline in order to develop the minimum albedo requirements for the cloud top surface models. The cloud top surface was assumed to be a boundary, and the infrared emissibity ε was set equal to 1-A where A was the value of the surface albedo. Integration of the reflected solar radiation over the spheres was done following the numerical algorithm discussed by Horak and Little (1965). In all the models, little variation was seen either in the narrow range of solar phase angles over which the observations were made, the average of which is 2°, or between this average and 0°. Therefore we assumed illumination at a phase angle of 0°.

We placed the boundary at the top of the convective region near 450 mbar. This is also close to the level of CH_4 condensation for the 0.2% CH_4 tropospheric mixing ratio case. The surface albedo required to match the 10.3 μm observation is 0.82 and implies an apparent geometric albedo for the planet of 0.042, considering reflected solar radiation alone (i.e. subtracting the thermal component). The low value of the geometric albedo with respect to the surface albedo is due to the two-way attenuation of the gaseous absorption at 10.3 μm. Fig. 5 shows the combined thermal and reflected solar radiation spectrum in terms of equivalent brightness temperature for a surface albedo constant with wavelength and with H_2 as the only gaseous absorber. This model fails to match the observed radiances at 11.6 and 12.5 μm, assuming a solar flux value taken from the mean of observations summarized by Vernazza et al. (1976) in their Fig. 11. This model also predicts radiances higher than the upper limits near 8-9 μm, observed by Gillett and Rieke (1977). However, if the reflecting cloud were composed principally of CH_4 ice crystals, a substantially darker surface albedo would result at these wavelengths due

to the increased ice absorption in the vicinity of the ν_4 vibration fundamental near 7.6 μm.

B. Neptune

The observations of Neptune reported here are illustrated in Fig. 6 together with the CVF and interference filter observations and upper limits reported by Gillett and Rieke (1977) and our recent observations at 17.8 and 19.6 μm (Tokunaga et al., 1982). The observation at 11.36 μm is consistent with the drop in emission on the short wavelength side of the ν_9 C_2H_6 band. Ostensibly, it is warmer than the observation of Gillett and Rieke at 11.3 μm. On the other hand, Gillett (personal communication) reports that their measurements at 11.3 μm could also be interpreted as a 3 standard deviation upper detection limit at 84.4 K. It is displayed as such in Fig. 6, consistent with the other upper limits displayed in the figure. Our attempt to detect Neptune at 10.90 μm was cut short by inclement weather, but Fig. 6 displays the appropriate (3 standard deviation) upper limit which is also consistent with the falloff in brightness temperature. As for the Uranus spectrum in Fig. 2, we also illustrate the brightness temperature equivalent to the radiance received from a sphere with a lambertian reflecting surface and characterized by various values for the geometric albedos.

Again, just as for Uranus, we make use of the hypothesis that all the radiation is thermal in origin. The shape of the drop in emission between the 11.5 μm Gillett and Rieke measurement and our 11.36 μm measurement, together with the 10.9 μm upper limit, suggest that the 10.3 μm brightness is not dominated by the short wavelength opacity of the ν_9 C_2H_6 fundamental. Thus, the 10.3 μm brightness most probably represents the measurement of a continuum level, as is the case with Uranus.

1. Temperature Structure

If, as for Uranus, the H_2 collision-induced dipole were assumed to be responsible for the atmospheric opacity at 10.3 μm, then the radiance measurement there could be used to constrain the temperature structure in the atmosphere of Neptune. We feel the need to emphasize that, without another measurement of the continuum brightness in the vicinity of 10.3 μm, the nature of the atmospheric opacity in this spectral region is purely an assumption, however plausible the analog with the spectrum of Uranus. In full knowledge of this caveat, however, we proceed with this assumption, if only to test predicted results against future observations in this region. Again, we assumed a bulk composition of 90% H_2 and 10% He and CH_4 by volume. The weighting functions associated with outgoing radiances at 10.3 μm and with 17.8 and 19.6 μm are quite close to those for Uranus under the same compositional assumptions. Therefore, we made direct temperature retrievals only at 60 and 400 mbar by perturbing one of Appleby's (1980) radiative-convective equilibrium models, repeating a procedure used by Tokunaga et al. (1982). Interpolation of temperature changes between 60 and 400 mb, perturbation of the stratospheric temperature structure, and modelling of the temperature structure for pressures greater than 400 mb were undertaken in precisely the same manner as for Uranus described in the preceeding section. The 0.1 mb temperature was also constrained to be roughly 140 K, consistent with the recent stellar occultation results reported by French et al. (1983).

As in the Uranus models (Fig. 2), the tropospheric CH_4 mixing ratio was set equal to 0.2%, 2% and 10% in three separate models, with CH_4 following saturation equilibrium above the condensation level. The presence of CH_4 in the stratosphere, as discussed below, had no discernable effect on the spectrum via the H_2-CH_4 collision-induced dipole owing to the much reduced pressures

involved and the pressure-squared dependence of this absorption. Although, we could not discriminate effectively among the three tropospheric CH_4 abundance models on the basis of our Neptune data alone, they should provide some utility via comparison with the Uranus spectrum with future observations of Neptune in this spectral region.

The results of the temperature retrievals are shown in Fig. 7 for each of the three CH_4 tropospheric mixing ratio assumptions. Fig. 6 illustrates the 8 to 20 μm brightness temperature spectra of the models, ignoring all opacities other than provided by the H_2 collision-induced dipole. All the models provide essentially equal quality in fitting the data, and all fit the 17.8 and 19.6 μm measurement well. As with Uranus, we also devised a hybrid model, modifying the slope of the temperature structure above the 60 mbar level until a fit to the 17.8 minus 19.6 μm brightness temperatures was achieved, and the 0.2% CH_4 model is plotted in Fig. 7. As in the case of Uranus, the spectra in the 8 to 20 μm region produced by the perturbed equilibrium vs. hybrid model are virvirtually indistinguishable with the present data.

2. Minor Constituents

Discrimination among the tropospheric CH_4 mixing ratio models cannot be made without other constraints on the "continuum spectrum" near 10 μm. For the purpose of provisional modelling of the stratospheric abundances of C_2H_6 and CH_4, we eliminated the 10% tropospheric CH_4 model by analogy with the Uranus modelling.

We computed spectra resulting when C_2H_6 is distributed vertically with nothing below the temperature minimum and the partial pressure equal to the vapor pressure in the stratosphere without exceeding the maximum mixing ratios shown in the figure. This distribution and the calculation of atmo-

spheric transmission followed the procedures used for the calculations of the C_2H_6 abundance in the stratosphere of Uranus described in the preceeding section. We note that Macy's (1980) synthetic spectra of the 11 to 13.5 μm region clearly indicate the influence of the ν_5 fundamental of C_2H_2 in the 13 to 15 μm range. Therefore we expect our models to produce brightness levels lower than those observed in the 13.0 to 13.5 μm region by Gillett and Rieke.

Fig. 8 displays the synthetic spectra of models with different values of the maximum stratospheric mixing ratio. A close match to the brightness at the center of the band is given by a maximum C_2H_6 mixing ratio just under 7×10^{-6} for the perturbed equilibrium model and 1.3×10^{-5} for the hybrid model. While this model appears to be significantly fainter than our measurement at 11.36 μm, the rise in blackbody intensity and brightness temperature with wavelength moves the effective wavelength of the CVF measurement from the nominal value of 11.36 μm to a value of 11.47 μm. This appears more than sufficient to reconcile the measurement with the stratospheric C_2H_6 mixing ratios which match the CVF measurements near the band center.

The influence of the ν_4 band of CH_4 is also shown in Fig. 8 for various stratospheric distributions using the same spectroscopic data base and computational scheme as for Uranus. CH_4 was distributed in the stratosphere so that its partial pressure was set equal to the saturation vapor pressure without exceeding the maximum mixing ratios shown in the figure; this is the same type of distribution used with C_2H_6 for both Uranus and Neptune. For either the perturbed equilibrium model or hybrid model temperature structures (Fig. 7), no satisfactory fit to the data is possible without exceeding a maximum stratospheric mixing ratio of 1×10^{-1}.

An increase in the temperature of the upper stratosphere in the perturbed equilibrium model as shown in Fig. 7 (short dashed line) produces only small changes in the 17.8 and 19.6 μm radiances, but allows the 8 μm spectrum to be fit with a maximum stratospheric mixing ratio of 4×10^{-2}. This increase in the temperature also implies a revision of the best fit maximum C_2H_6 mixing ratio from 7×10^{-6} to 3×10^{-6}.

3. Reflected Light

Reflecting-emitting cloud top models for Neptune were devised in the same way as for Uranus. Again, almost no difference in results was apparent between computations at the observational mean solar phase angle of 0.5° and computations at zero phase angle. Placing a cloud top boundary with unit albedo at the top of the convective region near 410 mbar and adding thermal emission from the atmosphere above the boundary fails to match the observed flux at 10.3 μm by a factor of 6. Nevertheless we recognized the possibility of higher level clouds from the recondensation of CH_4 descending from the warm stratosphere (see last section) which is consistent with reports of periodic brightning of Neptune, correlated at several infrared wavelengths, which indicates the inhomogeneous distribution of an upper level cloud (Joyce et al., 1977; Cruikshank, 1978; Brown et al., 1981). Therefore, we placed the boundary at the somewhat arbitrary location of 100 mbar at the very base of the thermally-inverted region in the temperature structures of Tokunaga et al. (1982). The surface albedo required to match the 10.3 μm observation is 0.70 and implies an apparent geometric albedo of 0.39, considering reflected solar radiation alone. Fig. 9 shows the combined reflected solar and thermal radiation spectrum in equivalent brightness temperature, if the surface albedo is constant with wavelength and H_2 is the only gaseous absorber. We note that

the emission features attributed to C_2H_6 at 12 μm and to CH_4 near 8 μm are well above the model spectrum. Just as for Uranus, if the reflecting cloud is primarily composed of CH_4 ice crystals, then a darker surface albedo and lower spectral intensities would be expected near 8 μm. Thus, it is probable that the radiances in the 8-9 μm region measured by Gillett and Rieke (1977) are almost entirely thermal in origin.

III. DISCUSSION

1. Thermal Contribution to the Spectrum

a. Tropospheric Temperatures

Serious systematic difficulties exist with the models presented here based on no contributions from reflected solar radiation. For both Uranus and Neptune, the temperatures near 400 mbars are several degrees warmer than Appleby's or other equilibrium models, or direct sensing models based on observations at longer wavelengths (see Figs. 15 and 17 of Trafton, 1981, for example). Furthermore, the models predict effective temperatures or brightness temperatures significantly in excess of several observations in the middle through far infrared (see Figs. 16 and 18 of Trafton, 1981). This strengthens the case for invoking reflected insolation as a significant component of the observed radiances.

Other possibilities deserve attention, however, and we cannot ignore the prospects of (a) systematic inconsistencies between our observations and those cited in the preceeding paragraph or (b) inappropriate assumptions as the basis for the thermal models. It is of obvious importance to check the consistency of the absolute calibration between 10-20 μm which are based on standard stars, and those at longer wavelengths which are usually based on thermophysical models for the Martian surface and atmosphere. Such a check might involve observations near 25 or 30 μm calibrated against the stellar standard system

along with an intercomparison of results with measurements based on other calibration systems.

b. Stratospheric Temperatures

The temperature structures of the perturbed equilibrium and the hybrid models of Uranus are substantially different in the 10 to 0.1 mbar region (Fig.3). Our modeling of CH_4 emission at 8 μm favored the lower temperatures of the hybrid model, maintaining consistency with CH_4 abundances cold-trapped by temperatures no lower than about 48K.

The revised temperature structure for Neptune (short dashed line in Fig. 7) is preferable to the hybrid model in order to reproduce the observed ν_4 CH_4 emission feature with plausible amounts of stratospheric CH_4. The upward change in the stratospheric temperatures by 10 K near 10^{-4} to 10^{-5} bars is consistent with the 140-155 K range determined by French et al. (1983b) near the 10^{-6} bar region. A change in the assumed stratospheric maximum mixing ratio of CH_4 would result from these temperature structure changes. For example, the warm stratosphere of Courtin et al. (1979) requires a constant CH_4 mixing ratio of only 4×10^{-3} to match the observations of CH_4 emission, but their profile gives a poor match to the 17.8 and 19.6 μm data of Tokunaga et al. (1983).

A cautionary comment is warranted, however, regarding the calculation of CH_4 or C_2H_6 emission in the upper stratospheres of either Uranus or Neptune. Our assumptions about the efficiency of stratospheric emission by CH_4 (as well as C_2H_6) could be incorrect. Appleby (1980) computed the source function for the ν_4 CH_4 band as dropping to 50% of the Planck function at roughly the level of 3×10^{-6} bars for all the outer planets. Reductions in the abundances of CH_4 and C_2H_6 with altitude owing to photochemical destruction, are also expected. For Jupiter, CH_4 and C_2H_6 both drop to a mixing ratio

of 2.5×10^{-5} near 0.01 mbar, according to Voyager UVS results (Atreya et al., 1981). These represent approximately 2×10^{-3} and 0.5 times their respective mixing ratios in the lower stratosphere. It is difficult to extrapolate such results to Uranus and Neptune in a way which is quantitatively meaningful. Our 0.1 mbar upper boundary for vertical integration of the outgoing radiance represents a first approximation to the combination of non-LTE emission and abundance depletion from photochemistry.

Finally, we do not expect clouds of CH_4 to change the outgoing stratospheric emission near 7 μm because the albedo of CH_4 ice particles is probably quite low. However, nothing is certain at this point. This especially true for Neptune, where CH_4 ice particles are more likely to be distributed in the lower stratosphere.

c. Minor Constituents

The abundance of CH_4 in the stratosphere of Uranus, as discussed earlier, is probably well represented by a mixing ratio equal to that at the temperature minimum, a value on the order of 3×10^{-5}. For Neptune, the CH_4 emission indicates that more is taking place: somehow CH_4 is migrating through the cold trap region. Whether this is taking place via "convective overshoot" which injects CH_4 into the warm stratosphere, upward eddy diffusion sufficiently strong to overcome gravitational sinking for very small particles of CH_4, or some other mechanism is not clear. The models show, however, that the observed emission is consistent with CH_4 distributed according to the local saturation vapor pressure, i.e. downwelling gas or an "inverted cloud". The value of the maximum mixing ratio of CH_4 in the warm stratosphere is dependent on the temperature structure assumed, but Fig. 8 illustrates that values of 1×10^{-2} to 1×10^{-1} are in the acceptable range, considering the observational uncertainties.

This probably implies a stratospheric mixing ratio which is roughly equal to that in the troposphere.

The abundance of CH_4 in the troposphere of Uranus is expected to be closer to 0.2 – 2% than to 10%, on the basis of residuals of the best fitting thermal model to our data. No such discrimination is available for Neptune because of our limited data. Further, any conclusions drawn indirectly from stratospheric abundances would depend on the efficiency of supplying CH_4 to the stratosphere from the troposphere.

2. Reflected Solar Contribution to the Spectra

The cloud models presented here are provisional and unsatisfactory in their simplicity. For a more complete physical model of the clouds, e.g. those for NH_3 ice clouds in the Jovian atmosphere (Marten et al., 1981; Orton et al., 1982), reliable indices of refraction for CH_4 should be used, due to the possible importance of ice absorption in the neighborhood of 7 μm.

If reflected solar radiation is a large component of the observed spectrum of Uranus near 10.3 μm, then Fig. 5 implies that either the thermal component at 11.6 and 12.5 μm is higher than that portrayed or that the reflectivity of the cloud must increase with wavelength in this spectral range. Such an increase could be due to an increase in the particle single scattering albedo associated with increasing distance from the 7 μm absorption feature, and it is less likely to be due to changes in scattering properties associated with the particle size or geometry over such a short wavelength range. Whether a cloud of CH_4 of optical thickness sufficient to provide the requisite reflectivity is consistent with constraints on the available CH_4 in the atmosphere remains to be tested; it is further complicated by the uncertainty in the tropospheric CH_4 content. In any case, the reflectivity of the atmosphere

in this spectral region is unlikely to be influenced by clouds at deeper levels owing to the rapid increase in H_2 opacity. In fact, this ensures that deeper levels are quite "dark". Particles of CH_4 or other bright materials, on the other hand, distributed at higher levels would be quite effective in increasing the atmospheric reflectivity.

For Neptune, detailed models of clouds must be more complicated, owing to the strong likelihood that clouds exist at or above the 100 mbar level, although probably they are distributed inhomogeneously across the face of the planet, as implied by studies at shorter wavelengths cited in the last section. Such clouds and hazes would be required to explain the observed 10.3 μm radiance, since radiation from deeper clouds is extinguished too efficiently by molecular H_2 absorption. While an effort could be made to observe the variability of the spectrum of Neptune in a search for the kinds of periodicity seen at shorter wavelengths, the observation times currently required for a single significant measurement cast great uncertainty on the effectiveness of this approach to produce meaningful results. In fact, thermal properties of the atmosphere could also be horizontally inhomogeneous. As for Uranus, higher clouds or bright particles would contribute effectively to a high planetary reflectivity.

We consider that the crude cloud models for Uranus and Neptune which are required to match the 10.3 μm observations are rather extreme in their reflectivity and optical thickness properties. It is difficult to make general statements in comparison with other wavelength regions without a quantitative physical model, but the near infrared part of the spectrum should be more susceptible to the presence of atmospheric particles. However, according to analysis of H_2 quadrupole lines near 1 μm (see the summary by Trafton, 1981), solar radiation does penetrate to and emerge from much deeper atmospheric

levels than permitted by our cloud top boundaries. A stronger case could be made for darker and optically thinner clouds if the thermal spectra were higher than shown in Figs. 5 or 9. This could arise from warmer temperatures in the 400 mbar to 1 bar region than implied by Appleby's (1980) models which form the basis for the temperature structures derived by Tokunaga et al. (1980) or from an abundance of He relative to H_2 significantly larger than the 10% to 90% ratio assumed here. We note that the assumption of normal H_2, rather than equilibrium H_2 as used in our models, would tend to decrease the thermal brightness in this portion of the spectrum.

d. Future Work

Much of the modeling work done here was not so much motivated by the information in the 5 new measurements presented in the second section as it was by the need to evaluate the best strategies for contraining the models most meaningfully by future observations and analysis. For Uranus and Neptune, observations at wavelengths below 10 μm will help to constrain the continuum, the thermal structure near 1 bar, and, by inference, the tropospheric CH_4 mixing ratio. If sufficient signal is available, a similar constraint can be accomplished via a relatively narrow band measurement of Neptune near 10.9 μm where the C_2H_6 emission should be negligible. Simultaneous analysis of new far infrared through millimeter data (Hildebrand et al., 1983; Nolt et al., 1983) should provide a highly synergistic assessment of the thermal structure as well.

The acquisition of new data for both planets in the 30 μm region with calibration to stellar standards should allow a check of the absolute flux determinations of longer wavelength obeervations in the same spectral region, e.g. new airborne measurements of both planets (Hildebrand et al., 1983; Moseley et al., 1983) which are referenced to a thermophysical model of Mars. A much improved evaluation of the thermal contribution to the 10-12 μm spectrum

would result. An increasing maturity of the H_2 collision-induced dipole absorption model and an evaluation of the influence of CH_4 and other types of particles of various sizes on outgoing thermal radiances should allow a more thorough evaluation of other source of systematic error.

More stringent upper limits to the CH_4 emission from Uranus and an addition of data longward of 8.3 μm and shortward of 8.0 μm for Neptune would place much better constraints on the stratospheric mixing ratio. Similarly, the determination of better constraints on the C_2H_6 emission from the stratosphere of Uranus would be provided by narrower band spectral observations near 12.2 μm. The extremely low flux involved in each of these observational requirements may predicate innovative techniques for spectral data acquisition, such as detector arrays, in order to avoid prohibitively long observational times. A confirmation of the uniformity of the CH_4 and C_2H_6 emission features of Neptune through the current time would also be prudent in order to ensure consistency with the 17.8 and 19.6 μm constraints.

ACKNOWLEDGEMENTS

This work was supported by NASA contract NASW 3159 (ATT), and NASA grant NSG 7320 (JC). GSO acknowledges the support of the Planetary Atmospheres Program of the NASA Office of Space Sciences and Applications for work carried out under NASA Contract NAS 7-100 at the Jet Propulsion Laboratory, California Institute of Technology. We gratefully acknowledge the IRTF observing staff, particularly C. Kaminski and R. Boehler, for their support in obtaining the data, and we acknowledge J. Hansen, N. Mehra, and D. Soll at the NASA Goddard Institute for Space Studies for computing support. We appreciate discussions with J. Appleby and K. Baines in the early stages of preparing this manuscript, we are indebted

to S. J. Kim for indicating modeling errors in an earlier version of this manuscript. We thank G. Birnbaum and L. Frommhold for laborstory results in advance of their publication as well as for numerous useful discussions. Finally, we are grateful for the constructive comments of L. Wallace and an anonymous referee in the reviewing process.

REFERENCES

Appleby, J. F. (1980). Unpub. Ph.D. Thesis, S.U.N.Y. at Stony Brook.

Atreya, S. L., T. M. Donahue, and M. C. Festou (1981). Jupiter: structure and composition of the upper atmosphere. Astrophys. J. 247, L43-L47.

Bachet, G., E. R. Cohen, P. Dore, and G. Birnbaum (1982). The translational-rotational absorption spectrum of hydrogen. J. Quant. Spectrosc. Rad. Transf. In press.

Baines, K. H. (1983). Interpretation of the 6818.9 Å methane feature observed on Jupiter, Saturn and Uranus. Icarus. In press.

Beckwith, S., N. J. Evans, E. E. Becklin, and G. Neugebauer. (1976). Infrared observations of Monoceros R2. Astrophys. J. 208, 390-395.

Birnbaum, G. (1982). Far infrared spectra of H_2 and mixtures of H_2-He and H_2-CH_4. In Vibrational-Rotational Spectroscopy for Planetary Atmospheres (M. Hunma, K. Fox and J. Hornstein, Eds.), NASA Conference Publication 2223, pp. 449-472.

Brown, R., D. P. Cruikshank and A. T. Tokunaga (1981). The rotation period of Neptune's upper atmosphere. Icarus 47, 159-165.

Cohen, E. R., L. Frommhold, and G. Burnbaum (1983). Analysis of the far infrared H_2-H_2 spectrum. Astrophys. J. In press.

Danielson, R. E. (1977). The structure of the atmosphere of Uranus. Icarus 30, 462-478.

Danielson, R. E., M. G. Tomasko, and B. D. Savage (1972). High resolution imagery of Uranus obtained by Stratosphere II. Astrophys. J. 178, 887-900.

Daunt, S. J., W. E. Blass, G. W. Halsey, K. Fox, R. J. Lovell, H. Flicker and J. D. King (1981). High resolution infrared spectrum and analysis of the ν_9 band of ethane at 12.17 μm. J. Molec. Spectrosc. 86, 327-343.

Dore, P., L. Nencinni, and G. Birnbaum (1982). Far infrared absorption in normal H_2 from 77 K to 298 K. J. Quant. Spectrosc. Rad. Transf. In press.

Fink, U. and H. P. Larson (1979). The infrared spectra of Uranus, Neptune and Titan from 0.8 to 2.5 microns. Astrophys. J. 233, 1021-1040.

Fink, W. and G. T. Sill (1982). The infrared spectral properties of frozen volatiles. In Comets (L. Wilkening, Ed.) Univ. of Arizona Press, Tucson, pp. 164-202.

Freeman, K. C. and G. Lyngå (1970). Data for Neptune from occultation observations. Astrophys. J. 160, 767-780.

French, R. G., J. L. Elliot, E. W. Dunham, D. A. Allen, J. H. Elias, J. A. Frogel, and W. Liller (1983a). The thermal structure and energy balance of the Uranian upper atmosphere. Icarus. In press.

French, R. G., J. H. Elias, D. J. Mink, and J. L. Elliot (1983b). The structure of Neptune's upper atmosphere: The stellar occultation of 24 May 1981. Icarus. In press.

Gautier, D. and R. Courtin (1979). Atmospheric thermal structure of the giant planets. Icarus 39, 28-45.

Gautier, D., B. Conrath, M. Flasar, R. Hanel, V. Kunde, A. Chedin, and N. Scott (1981). The helium abundance of Jupiter from Voyager. J. Geophys. Res. 86, 8713-8720.

Gautier, D., B. Bezard, A. Marten, J. P. Baluteau, N. Scott, A. Chedin, V. Kunde, and R. Hanel (1982). The C/H ratio in Jupiter from the Voyager infrared investigations. Astrophys. J. 257, 901-912.

Gautier, D., B. Conrath, M. Flasar, R. Hanel, V. Kunde, A. Chedin, and N. Scott (1983). The helium abundance of Saturn from Voyager. Preprint.

Gillett, F. C. and G. H. Rieke (1977). 5-20 micron observations of Uranus and Neptune. Astrophys. J. 218, L141-L144.

Hildebrand, R. H., R. F. Loewenstein, G. S. Orton, J. B. Keene, S. E. Whitcomb (1983). Observations of the Giant Planets in the 38-968 μm region: Implications for atmospheric structure and composition. In preparation.

Horak, H. G. and Little, S. J. (1965). Calculation of planetary reflection. Astrophys. J. Suppl. Ser. 11, 373-428.

Husson, N., A. Chedin, N. A. Scott, T. Cohen-Hallaleh and I. Berroir (1982). La banque de donnees "GEISA", Mise a jour no. 3 (Juillet 1982). Note Interne No. 116, Laboratoire de Meteorologie Dynamique de C.N.R.S., Ecole Polytechnique, Route Departmentale 36, 91120 Palaiseau Cedex, France.

Low, F. J. and G. H. Rieke (1974). The instrumentation and techniques of infrared photometry. In Methods of Experimental Physics, Vol. 12 (N. Carleton Ed.) pp. 415-462.

Macy, W. (1980). Mixing ratios of methane, ethane, and acetylene in Neptune's stratosphere. Icarus 41, 153-158.

Macy, W. and W. Sinton (1977). Detection of methane and ethane emission on Neptune but not on Uranus. Astrophys. J. 218, L79-L81.

Marten, A., D. Rouan, J.-P. Baluteau, D. Gautier, B. J. Conrath, R. Hanel, V. Kunde, R. Samuelson, A. Chedin, and N. Scott (1981). Study of the ammonia ice cloud layer in the equatorial region of Jupiter from the infrared interferometric experiment on Voyager. Icarus 46, 233-248.

Morrison, D. (1973). Determination of radii of satellites and asteroids from radiometry and photometry. Icarus 19, 1-14.

Moseley, H., B. J. Conrath, and R. F. Silverberg (1983). In preparation.

Nolt, I., J. Radostitz, G. Orton, P. Ade, C. Cunningham, and M. Griffin (1983). Submillimeter and millimeter observations of Uranus and Neptune. In preparation.

Orton, G. S. and A. G. Robiette (1980). A line parameter list for the ν_2 and ν_4 bands of $^{12}CH_4$ and $^{13}CH_4$, extended to J'=25 and its application to planetary atmospheres. J. Quant. Spectrosc. Rad. Transf. 24, 81-95.

Orton, G. (1981). Atmospheric structure of the outer planets from thermal emission data. In Infrared Astronomy (C. G. Wynn-Williams and D. P. Cruikshank, Eds.), pp. 35-53. D. Reidel Pub. Co., Dordrecht.

Orton, G. S., J. F. Appleby and J. V. Martonchik (1982). The effect of ammonia ice on the outgoing thermal radiance from the atmosphere of Jupiter. Icarus 52, 94-116.

Orton, G. S. and A. G. Robiette (1982). Errata: A line parameter list for the ν_2 and ν_4 bands of $^{12}CH_4$ and $^{13}CH_4$, extended to J'=25 and its application to planetary atmospheres. J. Quant. Spectrosc. Rad. Transf. 27. In press.

Orton, G. S. (1983). Thermal infrared constraints on ammonia ice particles as candidates for clouds in the atmosphere of Saturn. Icarus 53, 293-300.

Rieke, G. H. and F. J. Low (1974). Infrared measurements of Uranus and Neptune. Astrophys. J. 193, L147-L148.

Sicardy, B., M. Combes, A. Brahic, P. Bouchet, C. Perrier, and R. Courtin (1982). The 15 August 1980 occultation by the Uranian system: Structure of the rings and temperature of the upper atmosphere. Icarus 52, 454-472.

Simon, T., D. Morrison and D. P. Cruikshank (1972). 20-micron fluxes of bright stellar standards. Astrophys. J. 177, L17-L20.

Tokunaga, A. T., G. S. Orton and J. Caldwell (1983). New observational constraints on the temperature inversions of Uranus and Neptune. Icarus. 53, 141-146.

Trafton, L. M. (1967). Model atmospheres of the major planets. Astrophys. J. 147, 765-781.

Trafton, L. (1981). The atmospheres of the outer planets and satellites. Rev. Geophys. and Space Phys. 19, 43-89.

Vernazza, J. E., E. H. Avrett, and R. Loeser (1976). Structure of the solar chromosphere. II. The underlying photosphere and temperature minimum region. Astrophys. J. Supp. Ser. 30, 1-60.

Wallace, L. (1977). On the 1968 occultation of BD-17°4388 by Neptune. Astrophys. J. 197, 257-261.

Wallace, L. (1980). The structure of the Uranus atmosphere. Icarus 43, 231-259.

Ziegler, W. T. (1959). The vapor pressures of some hydrocarbons in the liquid and solid state at low temperatures. National Bureau of Standards Technical Note No. 4 (PB 151363).

APPENDIX

A Provisional Model for H_2-CH_4 Absorption

The H_2-He collision induced dipole absorption has been fit by Cohen et al. (1983) with

$$S_i = 33.53 \text{ K } A^6 \text{ (T/77.4 K)}$$

$$\tau_{1i} = 3.43 \times 10^{-14} \text{ sec (T/77.4 K)}^{1/2}$$

$$\tau_{2i} = 6.56 \times 10^{-14} \text{ sec (T/77.4 K)}^{1/2}$$

for the isotropic overlap dipole component and

$$S_q = 12.06 \text{ K } A^6 \text{ (T/77.4)}^{0.57}$$

$$\tau_{1q} = 8.94 \times 10^{-14} \text{ sec (T/77.4 K)}^{-0.60}$$

$$\tau_{2q} = 3.02 \times 10^{-14} \text{ sec (T/77.4 K)}^{-0.90}$$

for the anisotropic dipole (consisting of quadrupole and overlap components). These terms are explained in detail by Cohen et al. (1983).

We have perturbed these expressions to fit the available data for H_2-CH_4 collision-induced absorptions at 195 K and 297 K in the 20 to 900 cm^{-1} range and used the fit in the calculations presented in the text. Our best fit for H_2-CH_4 is obtained by the following expressions, similar to those for H_2-He

$$S_i = 648 \text{ K } A^6 \text{ (T/195)}^{0.14}$$

$$\tau_{1i} = 2.16 \times 10^{-14} \text{ sec (T/195)}^{-0.5}$$

$$\tau_{2i} = 3.00 \times 10^{-14} \text{ sec (T/195)}^{-0.5}$$

$$S_q = 223 \text{ K } A^6 \text{ (T/195)}^{-0.30}$$

$$\tau_{1q} = 9.55 \times 10^{-14} \text{ sec (T/195)}^{-0.5}$$

$$\tau_{2q} = 4.40 \times 10^{-14} \text{ sec (T/195)}^{-0.5}.$$

Table I

Absolute Flux Densities for α Boo

Effective Wavelength (μm)	FWHM Bandpass(μm)	x 10^{-15} W cm^{-2} μm^{-1}
10.3	1.3	1.93
10.90	0.16	1.66
11.36	0.17	1.42
11.6	1.3	1.30
12.5	1.2	1.05

Table II

Surface Brightness of Uranus and Neptune[a]

λ (μm)	x 10^{-10} W cm^{-1} μm^{-1} sr^{-1} July 1981	July 1982	Apparent Brightness Temperature (K)	Apparent Geometric Albedo
URANUS				
10.3	----------	6.55±1.69	$74.0^{+0.9}_{-1.1}$	0.039±0.010
11.6	----------	6.06±0.98	$67.7^{+0.5}_{-0.7}$	0.052±0.008
12.5	8.81±1.57	----------	$65.4^{+0.6}_{-0.7}$	0.115±0.020
NEPTUNE				
10.3	1.56±2.9	----------	$77.6^{+0.}_{-0.}$	0.229±0.043
10.90(CVF)	----------	10.0±17.5	<80.0(3σ)	<0.87(3σ)
11.36(CVF)	----------	102.1±16.4	$81.0^{+0.8}_{-0.9}$	2.10±0.34

[a]Assuming an equatorial radius of 25,900 km for Uranus (Dar[illegible]n, et al., (1972) and 24,800 km for Neptune (Freeman and Lyngå, 1970)

Figure Captions

Fig. 1 Filter transmission for the 10.3, 11.6 and 12.5 μm filters. The transmission was measured at room temperature, then shifted by 1.5% to shorter wavelengths to take into account the change in wavelength when the filter is used at liquid nitrogen temperatures. The estimated transmission of the terrestrial atmosphere above the IRTF is included in the transmission function.

Fig. 2 Brightness temperature spectrum of Uranus from 8 to 20 μm. Filled circles represent 3σ upper detection limits of Gillett and Rieke (1977). Circles with central point represent data of Tokunaga et al. (1982). Open circles represent data reported here. Vertical bars represent 1σ uncertainties when larger than the circles. Horizontal bars are schematic representations of the FWHM of interference filters. Model spectra, considering H_2 opacity alone, are represented by curves for various volume mixing ratios of CH_4 in the deep atmosphere: 0.2% (long dashed), 2% (solid), and 10% (short dashed). Thin solid lines represent the apparent brightness temperatures corresponding to values of geometric albedo, g, as marked.

Fig. 3 Temperature structures for Uranus derived in this work. Perturbations of an equilibrium model temperature structure from Appleby (1980) are shown, for various CH_4 mixing ratios in the deep atmosphere: 0.2% (long dashed), 2% (solid), and 10% (short dashed). A hybrid of the equilibrium structure and an ad hoc form above the 250 mbar level is shown for 0.2% CH_4 mixing ratio (alternating long and short dashed).

Fig. 4 Model spectra for Uranus in the 8 to 14 μm region for the perturbed equilibrium model with 0.2% CH_4 in the deep atmosphere. Solid curves represent model spectra (1.5% resolution) for various maximum mixing ratios of stratospheric C_2H_6: 3×10^{-8}, 1×10^{-8} and 3×10^{-9} (upper to lower), and stratospheric CH_4: 3×10^{-5}. The dotted curve represents the spectrum in the absence of stratospheric C_2H_6 or CH_4.

Fig. 5 Brightness temperature spectrum of Uranus from 8-20 μm, assuming the perturbed equilibrium model of Tokunaga et al. (1983). Filled and open circles have the same meaning as in Fig. 2. The lower curve represents the model spectrum from thermal emission alone with no lower boundary. The upper curve represents the spectrum from combined thermal emission and reflected sunlight from a model with a lower boundary at 450 mbar with a constant reflectivity of 0.82 (emissivity of 0.18), matching the 10.3 μm observations. Both model spectra assume atmospheric opacity due only to H_2.

Fig. 6 Brightness temperature spectrum of Neptune from 8 to 20 μm. Filled circles represent data of Gillett and Rieke (1977). Symbols have the same meaning as in Fig. 2, with upper detection limits representing 3σ noise levels and model spectra considering H_2 opacity alone with various tropospheric volume mixing ratios for CH_4: 0.2% (long dashed), 2% (solid), and 10% (short dashed). Thin solid lines represent the apparent brightness temperature corresponding to values of geometric albedo, g, as marked.

Fig. 7 Temperature structure for Neptune derived in this work. Perturbations of an equilibrium model temperature structure from Appleby (1980) are shown for various mixing ratios of CH_4 assumed in the deep atmosphere in the same way as Fig. 3. A hybrid of the equilibrium structure and an ad hoc form above the 200 mbar level is also shown for a 0.2% CH_4

mixing ratio, also denoted as in Fig. 3. A warm upper stratosphere alternative to the perturbed equilibrium model is shown by the short dashed line for pressures less than 10 mbar.

Fig. 8 Model spectra for Neptune in the 8 to 14 μm region for the perturbed equilibrium model with warm upper stratosphere. Models for a tropospheric CH_4 volume mixing ratio of 0.2% are shown. Solid curves represent model spectra (1.5% resolution) for various maximum mixing ratios of stratospheric C_2H_6: 1×10^{-5}, 3×10^{-6} and 1×10^{-6} (upper to lower) and stratospheric CH_4: 1×10^{-1}, 4×10^{-2} and 2×10^{-2}. The dotted curve represents the spectrum in the absence of C_2H_6 or CH_4.

Fig. 9 Brightness temperature spectrum of Neptune from 8-20 μm, assuming the perturbed equilibrium model of Tokunaga et al. (1982). Filled and open circles have the same meaning as in Fig. 6. The lower curve represents the model spectrum from thermal emission alone with no lower boundary. The upper curve represents the spectrum from combined thermal emission and reflected sunlight from a model with a lower boundary at 100 mbar with a constant reflectivity of 0.70 (emissivity of 0.30), matching the 10.3 μm observation. Both model spectra assume atmospheric opacity due only to H_2.

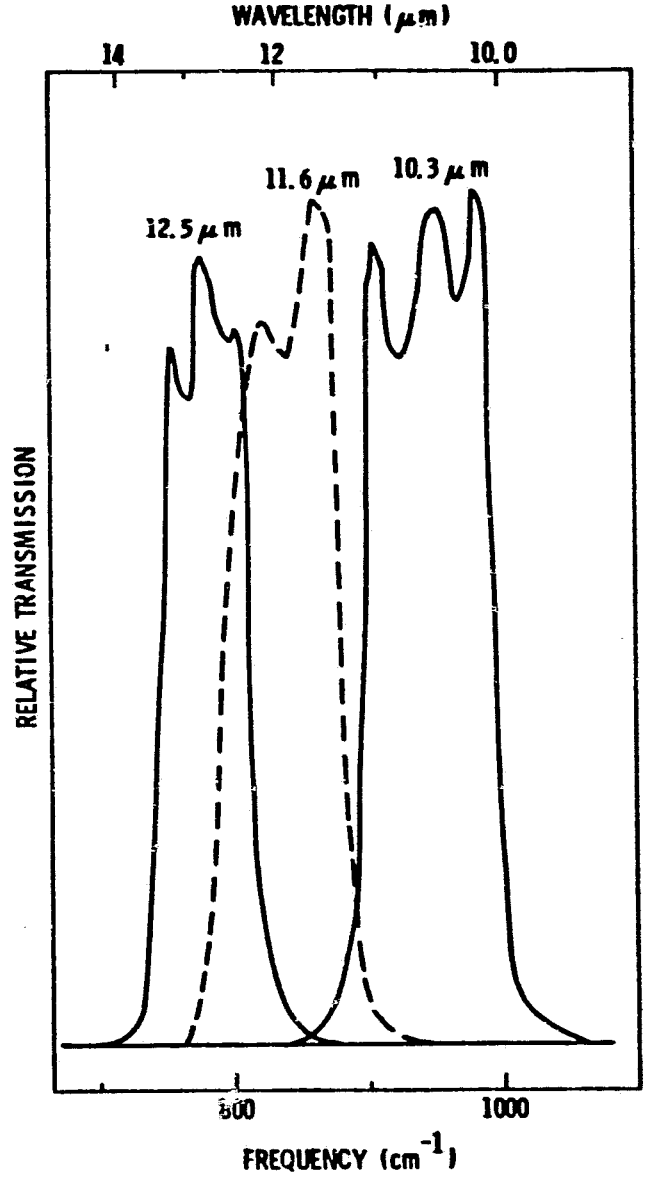

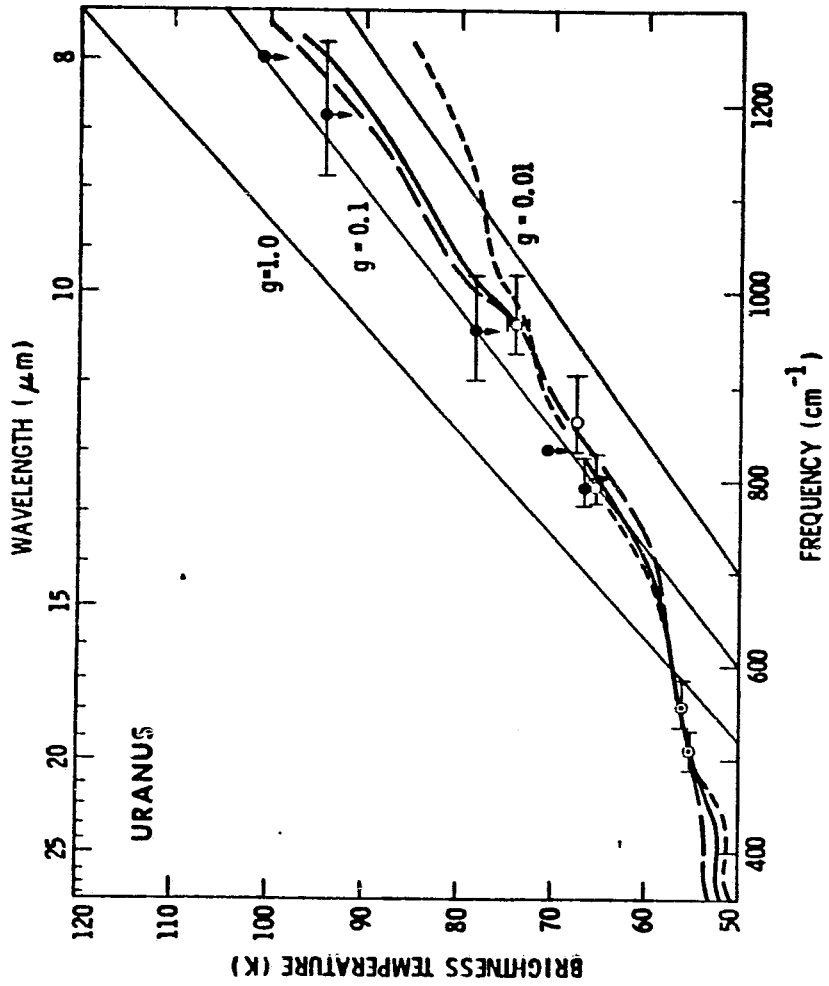
URANUS
g=1.0
g = 0.1
g = 0.01
WAVELENGTH (μm)
FREQUENCY (cm⁻¹)
BRIGHTNESS TEMPERATURE (K)
8
10
15
20
25
1200
1000
800
600
400
120
110
100
90
80
70
60
50

Figure 2

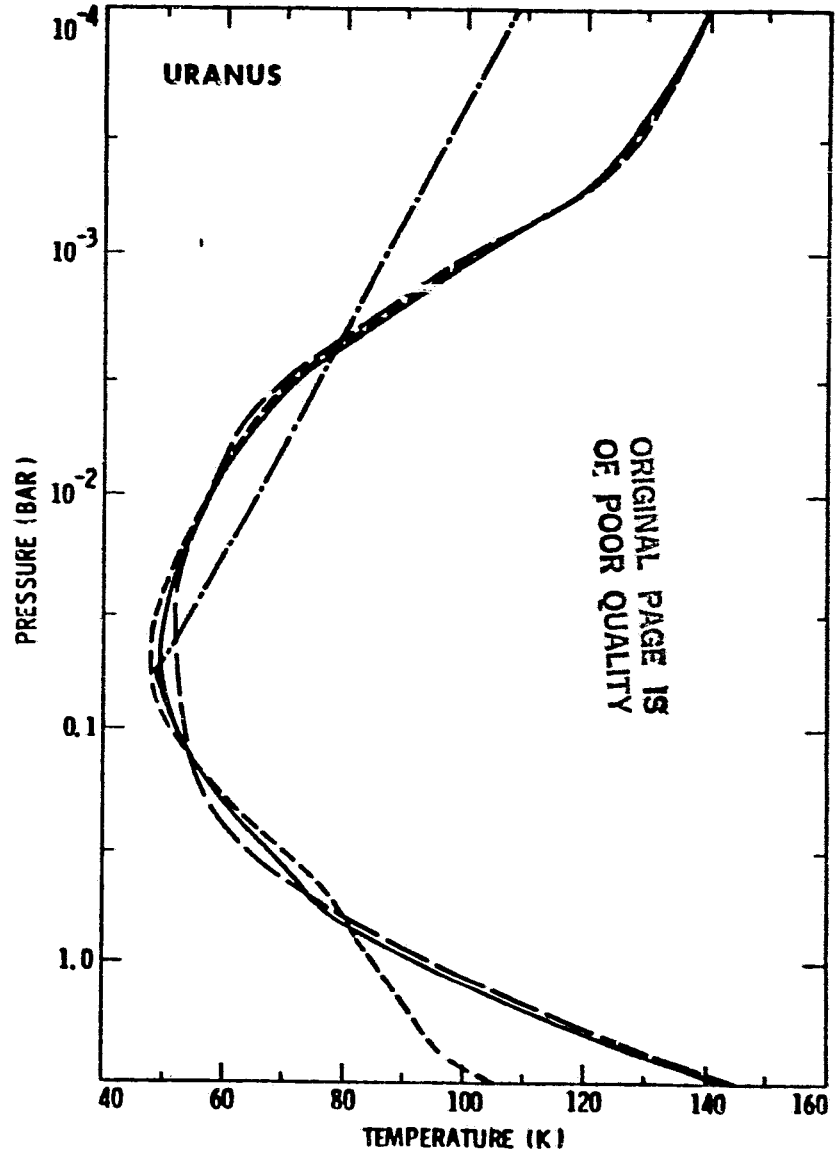
URANUS
PRESSURE (BAR)
TEMPERATURE (K)
10⁻⁴
10⁻³
10⁻²
0.1
1.0
40
60
80
100
120
140
160
ORIGINAL PAGE IS
OF POOR QUALITY

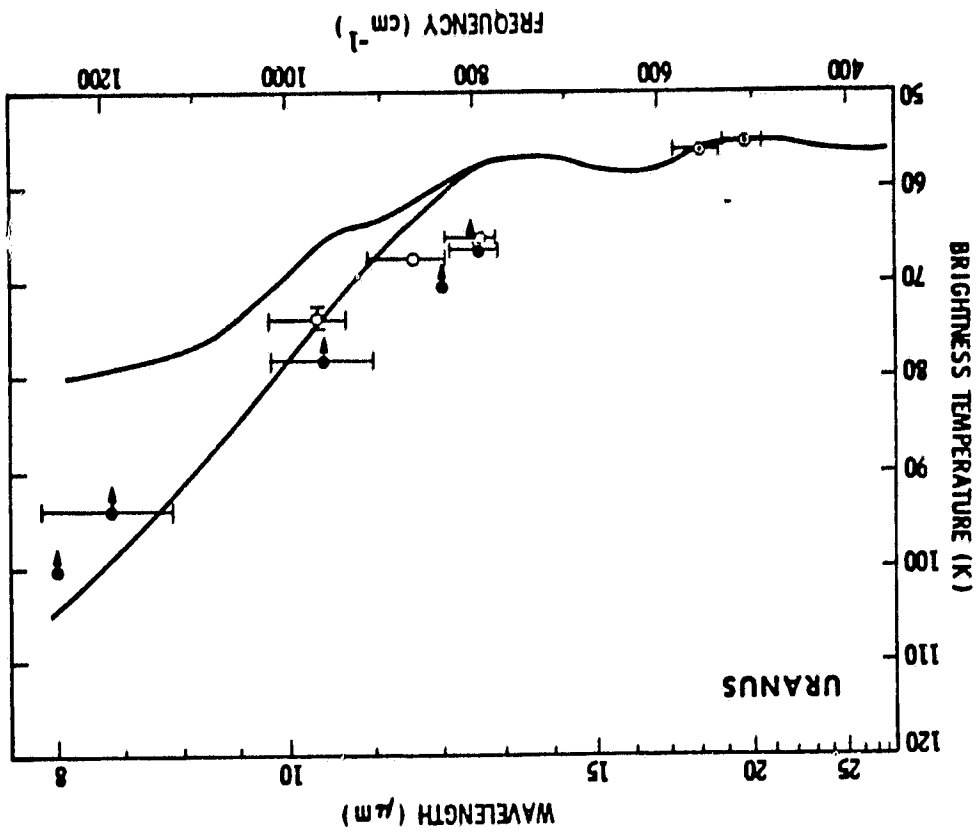

Figure 5

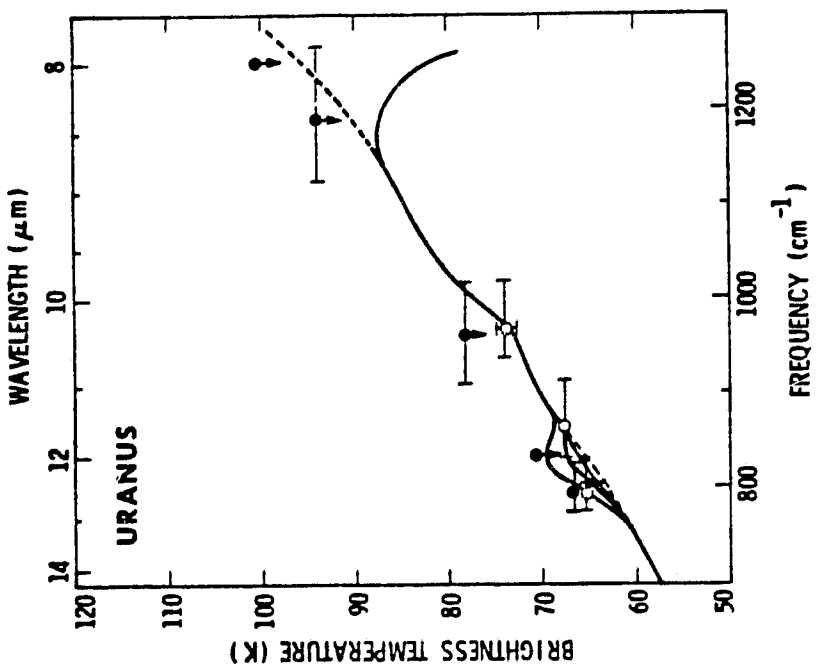

Figure 4

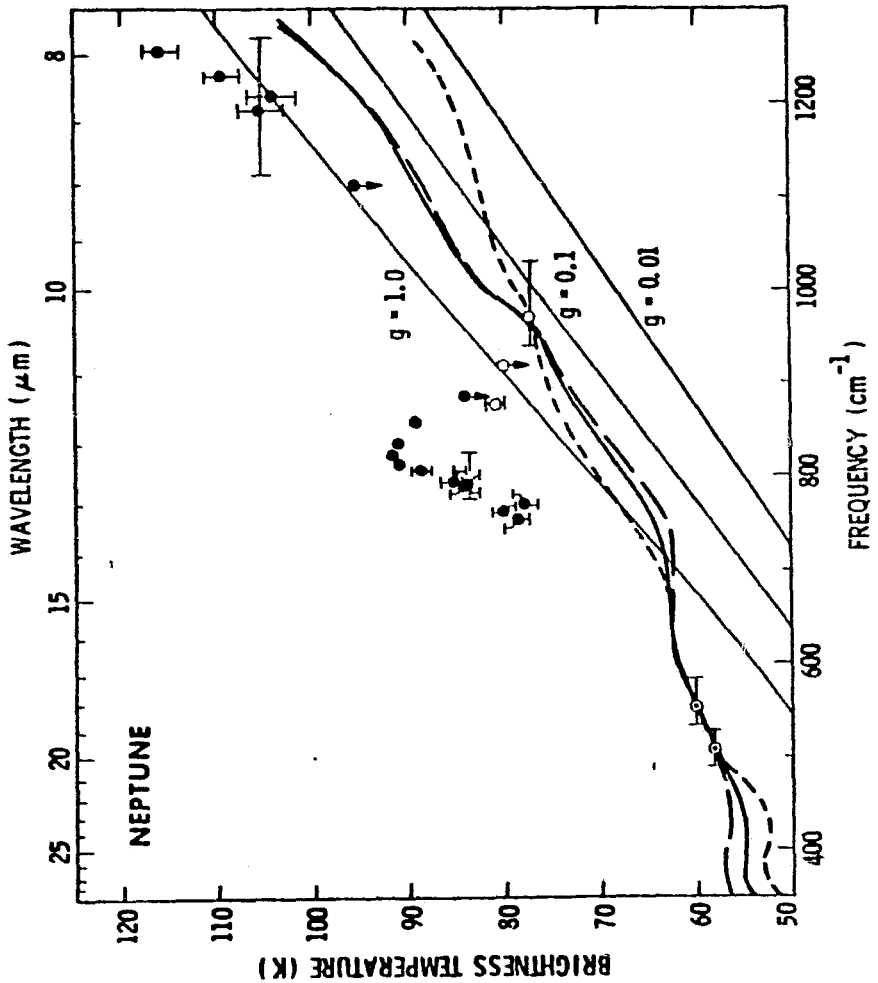

Figure 6

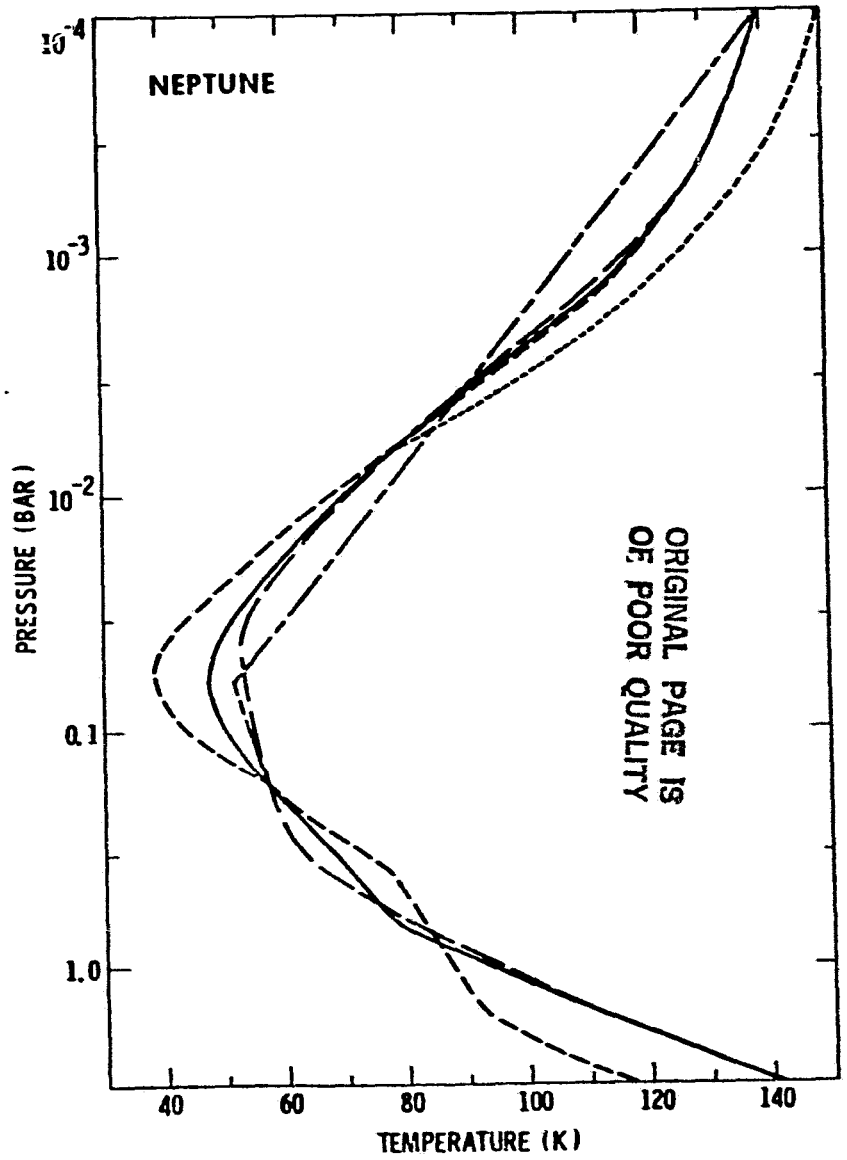

Figure 7

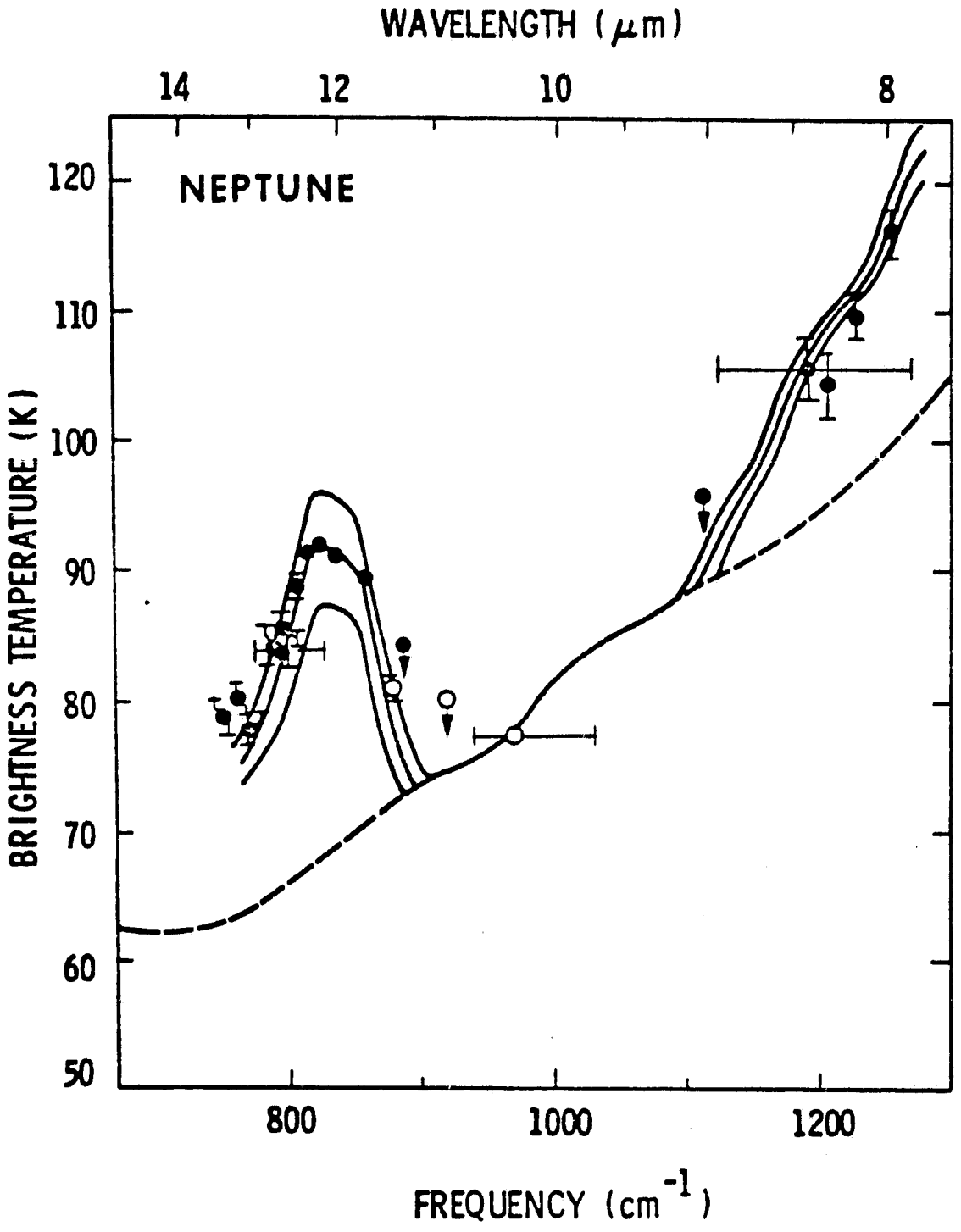

Figure 8